ՀԱՅԱՍՏԱՆԻ ՀԱՆՐԱՊԵՏՈՒԹՅԱՆ ԳԻՏՈՒԹՅՈՒՆՆԵՐԻ
ԱԶԳԱՅԻՆ ԱԿԱԴԵՄԻԱ
НАЦИОНАЛЬНАЯ АКАДЕМИЯ НАУК РЕСПУБЛИКИ
АРМЕНИЯ

Հայաստանի քիմիական հանդես 60, №2, 2007 Химический журнал Армении

INTRINSIC STRUCTURAL-BALLISTIC INTERACTIONS IN COMPOSITE ENERGETIC MATERIALS

PART I - EXPERIMENTS

G. SANDRI TUSSIWAND[a], F. MAGGI[b], A. BANDERA[a] and L.T. De LUCA[c]*

[a] PhD candidate, SPLab, Politecnico di Milano, 34 via La Masa, 20158 Milan, Italy
[b] PhD, SPLab, Politecnico di Milano, 34 via La Masa, 20158 Milan, Italy
[c] Professor, SPLab, Politecnico di Milano, 34 via La Masa, 20158 Milan, Italy

* luigi.deluca@tiscali.it

ABSTRACT

Among the various aspects of the deflagration of composite solid rocket propellants, one deserving further attention is the dependence of the propellant regression rate on its mechanical state, properties and applied loads during deflagration. Beside structural-ballistic interaction phenomena occurring on a motor level, i.e. affecting the whole grain or large portions of it, the structural properties of a propellant and the mechanical loads acting during deflagration can significantly alter its combustion behavior on a microscopic scale, leading to what can be considered as an “intrinsic” coupling mechanism. This can affect the performance of a solid rocket motor even without the presence of macroscopic cracks or excessive grain deformation, and has been the subject of several experimental and theoretical investigations performed at the SPLab (Space Propulsion Laboratory) of Politecnico di Milano on AP-HTPB based composite propellant formulations. The same mechanism could also alter the IM properties of an energetic material which has been subjected to mechanical damage and chemical aging.

Nomenclature

a	*thermal diffusivity or crack length*
a’	*rate of crack propagation*
E	*Stiffness*
E(t)	*relaxation modulus in tension*
G	*Cross flow in the bore*

$g(\varepsilon)$	*Strain softening function – Swanson & Christensen's NLVE model*
H/C	*Hydrocarbon*
k	*thermal conductivity*
LVE	*Linear viscoelastic material model*
IM	*Insensitive Munition (here mainly slow and fast cookoff)*
NLVE	*Non-linear viscoelastic material model*
PBX	*Plastic bonded explosive*
q	*thermal energy flux*
r_b	*burning rate*
T	*Temperature*
t	*Time*
T_f	*Final flame temperature*
T_s	*surface temperature*
T_0	*soak temperature*
ε'	*strain rate*
ε	*Strain*
λ	*Average size of the largest particles in a propellant*
ρ	*density*
σ	*Stress*

Introduction

Global structural-ballistic interactions on a motor level are those which alter significantly the expected burning behavior of the grain either through excessive deformation of its geometry or through crack propagation in the grain and the associated generation of additional burning surface. They have detrimental effects on the thrust and pressure histories of the complete motor and may cause catastrophic failure of the system.

Another kind of structural-ballistic interactions, which can be denoted as "intrinsic", are those influencing the speed of deflagration of the propellant itself. Their effect is on a microscopic scale, without any occurrence of structural collapse of the grain by crack generation and propagation or excessive deformation. Their triggering cause is mechanical damage, particularly the presence of porosity, kept open by a tensile stress/strain field and generated by mechanical damage on a microscopic scale, i.e. adhesive fracture between the solid particles and the binder or cohesive fracture in the binder itself. This mechanism, known as dewetting, can increase the apparent burning rate of the material.

Intrinsic structural-ballistic interactions are difficult to investigate on a laboratory scale because of the need to keep burning material samples under a constant mechanical load. The amount of burning rate increase caused by mechanical damage seems to be pressure dependent on a sample level; mechanical damage will therefore alter the apparent ballistic exponent of a propellant on a laboratory scale.

The intrinsic interaction effect inside a motor will generally be different: the presence of damage-induced porosity enhances the feedback of thermal energy in depth into the material not only by conduction, but also by radiation and convection; the influence of the two latter mechanism will be dominant inside a grain but seems difficult to reproduce using small propellant samples. For a motor, even neglecting convection, the mere high radiant energy flux emanating from the bore can produce subsurface ignition of smaller oxidizer particles [1], accelerating bulk deflagration. Finally, the coupling of damage-induced porosity and other burning rate enhancing effects such as erosive burning will also contribute to change things on a motor level.
IM properties of the grain, like its sensitivity to fast and slow cook-off aggressions, might also be altered, changing its overall response to aggressions after cumulative mechanical damage evolved in open porosity.
Activities on the intrinsic interaction effect involved the investigation of the rate of regression of damaged AP-Al-HTPB propellant under mechanical strain and the modeling of the experiments.

So far, the following results have been obtained:

– For materials containing a bonding agent, the regression rate is significantly altered if the applied level of tensile strain exceeds the onset of dewetting between AP particles and the binder. The variation of burning rate is then a <u>“fingerprint” of the state of damage of the material.</u>

– Since the material is not homogeneous, any induced strain field will produce a non homogeneous distribution of damage and load on a microscale. This implies that a bit of material will have a non-homogeneous distribution of burning rate. Experiments on damaged propellant slabs under strain showed indeed an enhanced generation of vorticity on a microscopic level, particularly at spots where the damage distribution was highly inhomogeneous. This means that the “combustion noise” is greatly enhanced in material portions with damage level gradients.

– If the material does not contain an effective bonding agent (e.g. formulations based on nitramines and binder, new formulations for space launchers, PBX, etc.), a progressive increase of the burning rate with the applied strain is to be expected [2]. In this case, the variation of burning rate would be a “fingerprint” of the superposed strain field and will be influenced by the original, specific microscopic structure of the material and by the nature of its constituents.

– The increased mass burning rate is caused by an increased burning surface on a microscopic level. For the samples, debonded AP particles ignite below the “reference” burning surface through conduction in the gas phase between the debonded particles and the binder matrix. This effect would be enhanced and virtually independent on pressure in a motor because of the intense convective and radiant thermal energy exchange.
Part 1 of this work describes the experiments performed on damaged propellants with and without load application. Part 2 [30] describes some simple modeling activities performed to confirm the

physical explanations proposed after observing the experiments and to help understanding the phenomena involved. A correlation between the amount mechanical damage and burning rate augmentation is also suggested.

Literature Survey

Failures caused by global structural-ballistic interactions have been investigated in the past, with much effort occurring in the US after the Titan IV SRMU prequalification test failure on the 1st of April 1991. Material focusing on global collapse caused by excessive deformation and a review of previous work published on the subject in the USA is offered in [3]; a similar, full-scale failure occurred during a Castor II motor firing had been investigated and modeled by Glick, Caveny and Thurman in 1967 [4].
Another valid survey has been published in [5]. Simulations including excessive deformation and the spontaneous initiation and propagation of a crack inside a motor have been recently published by one of the workgroups of the CSAR program at the University of Illinois (e.g., [6]). Previously, a considerable amount of work on failure caused by crack initiation and propagation was carried out by Smirnov and Dimitrienko [7] in the former Soviet Union, and after that in the USA at the Pennsylvania State University by Kumar, Kuo, Lu and others (e.g., [8] and [9]) in the 80s and 90s and by Liu at the Edwards AFB laboratory [10].
Some early material on the intrinsic effect of load and damage on the ballistic properties of a solid propellant was found in [2]. Two of the studies quoted here could not be found, but report intrinsic structural-ballistic interaction as a function of the strain. The authors' comment stresses that the cause of the burning rate acceleration under strain is unclear but suspects dewetting to be the triggering mechanism.
Useful modeling activities or experimental studies are scattered in literature ([5] and [10], for instance), but no dedicated study was found so far.

Material

The composite propellant used in this study belongs to the most employed family used for solid rocket propulsion applications in the western countries. It is a heavily filled elastomer, containing a distribution of rigid AP particles as oxidizer and metal particles as fuel. They make up about 90% of the mass. The binder works as a fuel and is a polyurethane elastomer, using HTPB as base polymer, networked through a polyfunctional isocyanate. Further additives play a fundamental role in determining the mechanical properties of the compound: the plasticizer is an organic oil depositing itself between the binder chain segments, facilitating mutual shearing through weakening of the van-der-Waals bonds existing between different atoms of the chain segments, and the bonding agent is a “hybrid” molecule, containing functional groups capable to react both with the rigid, inorganic AP particles and the binder, thereby establishing strong bonds between the rigid inclusions and the binder itself.

The organic molecules of the binder decompose during combustion and react with the oxidising gases generated by the primary AP flame [11-12], producing a diffusion flame and releasing further thermal energy to sustain stable flame propagation into the solid.

The following formulations were investigated:

– A formulation having a ratio of AP:Aluminum:binder of about 68:18:14, a bimodal AP grain size distribution with peaks at 20 μm and 200 μm and an average Aluminum grain size of 30 μm. Ferric oxide was used as a burning rate modifier. This propellant comes from an industrial batch and the indications are approximate. It contained an effective bonding agent and will be referred to as ***formulation 1***.

– A very similar formulation, using a finer AP powder, less Aluminum, a different burning rate modifier and a higher bonding agent and plasticizer content, giving better strain capability, a later onset of dewetting and an excellent toughness. From the point of view of this study it is similar to formulation 1. Both are typical of good quality, industrial grade propellants.

– A self-produced fuel-rich formulation, having a ratio of AP:binder:Aluminum of about 60:20:20, a bimodal AP grain size distribution with peaks at 80 μm and 200 μm, the Aluminum having an average grain size of 70 μm. The saturation degree of the binder was 100%, the propellant contained no bonding agent and less plasticizer than above. As a result, the material was very brittle, exhibiting a very early onset of dewetting, and will be referred to as ***formulation 2***.

Experiments

A number of different experiments was designed and carried out to investigate the effect of mechanical damage and load on the burning rate of the energetic material.

Burning rate measurements were performed on undamaged and damaged material, using conventional Crawford samples cut out of dogbone specimens used for uniaxial tensile testing and panels previously loaded under biaxial tensile stress [13]. Obviously, no tensile load was applied to the strand burners during combustion.

Further burning rate measurements were performed with special panel samples loaded in plane stress during burning. The material of these samples belonged to formulation 1 and was cut out of subscale ballistic simulation motors; it was subjected to controlled mechanical damage before the burning rate experiments.

Mechanical characterisation of propellant formulation 1 was performed a priori following the LVE and the Swanson model in order to provide data for the structural analysis of the burning rate specimens and on the onset and amount of microstructural damage in the material.

Irreversible damage in a composite propellant

With damage onset we mean the strain at which truly irreversible damage occurs in the propellant. Other forms of changes in the material's microstructure, like the Mullin's effect, have relevant consequences on its mechanical properties and pose challenges to constitutive modeling [14, 25-28], but do not seem to be completely „irreversible".

Leaving out the Mullins effect and other long-term mechanisms altering the material, like oxidative cross-linking caused by chemical aging, we just consider fully irreversible damage, i.e. modifications in the propellant caused by mechanically-induced destruction of stronger bonds in the binder or at the particles' interface, such as detachment of bonding agent molecules from the oxidizer particles and/or the binder producing "dewetting" [13 and 29].

The damage patterns observed in the heterogeneous energetic material are related to the size of the oxidizer particles and can be grouped into three types for the purpose of this study:

– Diffused microcracks/dewetting *(Fig. 1)*, a state of damage where many small fractures occur on a microscopic scale. They are as large as the largest solid particles or particle agglomerates in the propellant, in our case a few hundred microns. Depending on the temperature, the strain rate of the applied load, and the bonding agent effectiveness, the fracture can proceed near the particles [10;15-17] at stress concentration spots, or directly at the particle-binder interface. In the presence of a significant amount of metallic fuel particles one order of magnitude smaller than the larger oxidizer inclusions, we have dewetting of metallic fuel particles from the binder at even lower strains, i.e. a smaller fracture scale of a few tens of microns concentrated at the metal pockets between the larger oxidizer particles [18]. In all cases, the presence of plasticizer means that the particles which lost contact to the binder are, at least initially, partially or completely wetted with a volatile organic liquid.

– Small Bridged Cracks *(Fig. 2)*. Coalescence and propagation of the above microcracks at favourable spots to form a larger crack of the size of 2-3 large oxidizer particles (e.g. near an agglomerate of small metallic particles, or at a spot with a local enrichment of larger oxidizer particles with surface irregularities). Under load, the crack is still bridged by oriented binder filaments. The crack surface is punctuated by metallic fuel particles, large oxidizer grains and a number of small oxidizer particles, depending on the specific formulation of the propellant; all particles are, at least initially, wetted by plasticizer.

– Small open Cracks *(Fig. 3)*. Coalescence of the above structures and propagation of the bridged crack patterns described above to form a true crack, which can or cannot be considered to be "microscopic" depending on the scale of observation and on the available diagnostic technique; it might be "microscopic" or undetectable on a motor level if it is smaller than the resolution of an x-ray image, but it will be larger than a few of the bigger oxidizer grain particles. If loaded, the crack is not bridged by binder filaments for a significant portion of its length. Bridging will occur at the crack tips, within a so-called process zone [19].

A characteristic scale to define the damage pattern is the average length of the larger oxidizer particles or the largest agglomerates in the propellant, λ. For the formulations tested in this study, a damage pattern of the first kind has microcracks with $\mathbf{a \leq \lambda}$. A damage pattern of the second kind has bridged microcracks with $\mathbf{a \approx 2\text{-}3\ \lambda}$**,** and a damage pattern of the third kind has $\mathbf{a}$ > $\mathbf{3\text{-}4\ \lambda}$ **and**

up to 1-2 mm. If no tensile load is applied, the cracks close and a continuity in the material is re-established. Initially disconnected surface bits are held together by weak bonds (van der Waals forces) which collapse as soon as very small tensile loads are applied. The damaged material is not able to transmit the same amount of stress in a region of damage pattern 1 since porosity decreased the bulk stiffness causing softening.

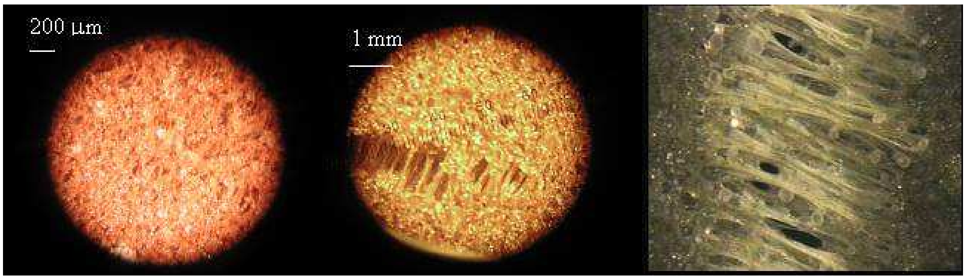

Fig. 1 *(left)* *Damage pattern 1: diffused oxidizer particle dewetting.* **Fig. 2** *(centre) Damage pattern 2: bridged crack propagated by a few AP particles. The larger particles are embedded in the bulk, so that in the gaps there is effectively a higher local concentration of small particles.* **Fig. 3** *(right) A crack shows all the previously described damage regions: a true crack, ending in a process zone (shown in the picture) beginning with a type 2 region ($\lambda \approx$ 2-3 large oxidizer particles) and ending in a type 1 region (dewetting, $\lambda \approx$ 1 large oxidizer particle).*

In a region like in Fig. 2, the amount of stress transmitted is even more limited, and due to the mere binder filaments bridging the crack surface. In a region of damage pattern 3 (true crack), no stress at all is transmitted except at the tips, in the process zone. The process zone itself has a variable size, depending on temperature and loading rate [19-20]. The initial portion (crack bridged by crazing filaments) is effectively a pattern 2 damage zone, and the final part (microcrack region) is a pattern 1 zone, with dewetting. A fracture in the propellant allows the observation of all three types of damage.

Burning rate measurements on damaged material without load application

To check whether a modification of the burning rate occurred in a damaged material, a preliminary investigation was performed using strand burners belonging to formulations 1 and 2. The strand burners were taken from damaged material samples stretched at 25°C and low strain rate (5 mm/min) to 30% and 5% true strain respectively and kept strained for at least one hour. Both strain levels cause irreversible damage in the material. Formulation 1 material was also loaded using a biaxial plate specimen [13] stretched to 30% true strain in the centre. At centre of the biaxial specimen, an almost equibiaxial state of tension damages the material producing microcracks in the direction of straining and at 90° to it because of incompressibility (the material's contraction is inhibited).

The material strands measured 5x5x30 mm and were tested at atmospheric pressure without load application. Ignition was produced using a hot wire, and the burning rate was measured using video recordings of the tests through a digital image processing methodology described in [21]. The results obtained were compared to similar measurements performed on undamaged material tested at the same temperature and pressure. Results are summarized in Table 1.

Formulation	State of the material	Loading condition	r_b, mm/s	Max. r_b, mm/s	COV	Remark
2	undamaged	unloaded	1.24	1.27	3.39%	Brittle
2	damaged	unloaded	1.44	1.60	15.8%	strained uniaxially[1]
1	undamaged	unloaded	1.16	1.19	1.82%	Taken from subscale analogs
1	damaged (g = 0.375), 30% true strain	unloaded	1.15	1.19	2.20%	Taken from subscale analogs, strained uniaxially[1]
1	damaged (g = 0.375), 30% true strain	unloaded	1.19	1.26	3.34%	Taken from subscale analogs,strained biaxially[2]

Table 1: *burning rates at 1 atm using mechanically damaged samples. The samples were unloaded during burning.*

A significant increase of the burning rate occurs for a damaged brittle formulation without bonding agent even if it is unloaded, in accordance with what is reported in [2].

No effect is recorded using an AP/HTPB formulation with good mechanical properties if the material is damaged through a tensile load producing significant dewetting in the direction of flame propagation (i.e. inducing microcracks parallel to the burning surface) and unloaded during burning, but there seems to be a slight increase in the average burning rate and the measurement dispersion if there is some amount of damage/microcracks produced at 90° to the burning surface, i.e. parallel to the direction of propagation. The increase in burning rate appears more clearly if one focuses on the maximum recorded values. A thorough examination of the test video recordings showed occasional subsurface ignition phenomena (Fig. 4) to be the reason for the average burning rate increase.

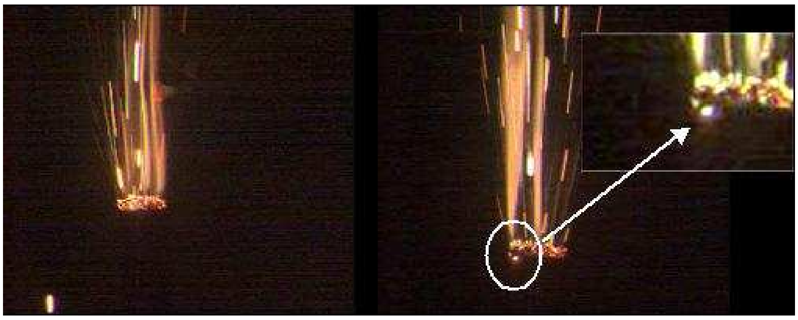

Fig. 4 ***Left:*** *burning surface of undamaged, formulation 1 samples.*
Right: *burning surface of samples taken from biaxial tensile specimens, showing accelerated deflagration through ignition below the main surface*

[1] Microcracks parallel to the burning surface
[2] Microcracks parellel and perpendicular to the burning surface

Even if the propellant is unloaded during burning, there seems to be thermal energy exchange below the main burning surface leading to subsurface ignition.

Burning rate measurements on damaged material under load

Propellant samples under load are more representative of the real conditions of the material in the inner part of a motor, at and near the bore surface [13, 22-23]: beside a state of hydrostatic compression generated by the gas pressure in the bore, the part of the grain at the bore is subjected to a tensile load because of the compliance of the case itself, which expands under the internal pressure generated by motor operation. If enhanced flame propagation was occurring through flame spreading into open microcracks, then keeping the material loaded during combustion was supposed to produce some burning rate acceleration effect.

To keep a propellant sample under a reasonably constant average tensile load during combustion, a 2D specimen and a special fixture were designed and manufactured. The sample is a propellant slab of 100x20 mm, 3-4 mm thick. It is held in position and strained using movable clamps with edge screws (see Fig. 5). The movement of the clamps is achieved through a frame made by 4 M3 screws and nuts. The clamps are pushed apart by adjusting the position of the screws and impose a stretching displacement to the propellant sample. Some white spots were drawn of the sample to measure the local tensile displacement under the microscope, and be sure that no slipping occurred at the frame. The average true strain imposed to the material is equal to

$$\varepsilon_{xx} = \ln\left(1 + \frac{\Delta W}{W_0}\right) \tag{1}$$

W_0 is the initial width of the sample between the fixture and ΔW is the displacement imposed to the frame. The distribution of strain is shown in the FEA described in the modelling section in part 2. Microcracks develop following the intrinsic heterogeneity of the material and propagate at spots with a higher concentration of large solid particles. When a crack forms, the material nearby is unloaded except at the two tips of the crack. This means that damage will tend to "nucleate" at spots with a higher concentration of larger oxidizer particles and its distribution won't be uniform. Since the specimens had been previously strain cycled beyond the onset of dewetting, the true tensile stress and strain distribution depends on the damage pattern generated during the strain cycling and is not reproducible even if the imposed average strain was the same for all specimens.

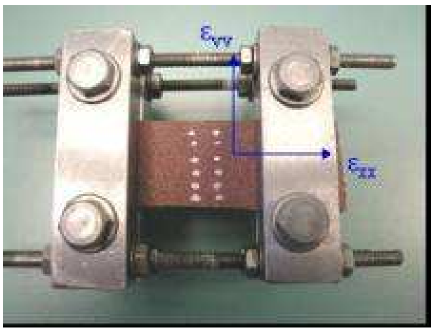

Fig. 5 *Fixture and 2D propellant samples to measure the burning rate under load*

While loaded, the samples were ignited by a hot wire placed on a stripe of black powder on the upper edge. All samples were burned in nitrogen and were inhibited at the outer surface.

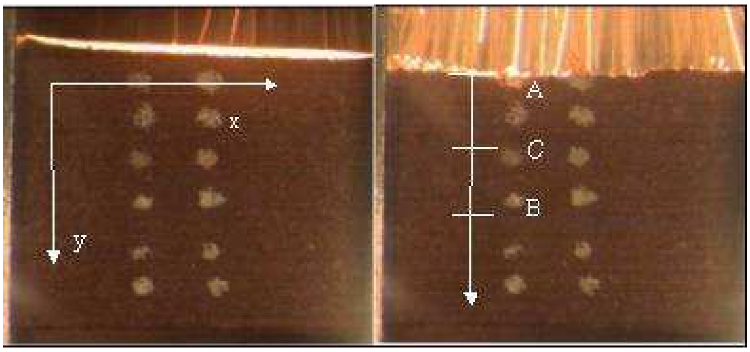

Fig. 6 *Ignition of the sample through a hot wire on the top and burning surface advancement from top to bottom during the experiment. The arrow shows the local propagation direction*

The burning rate of the material was measured through digital image analysis of the *local* burning front position via the software of the camera used to film the experiments.

A 2D burning rate field was obtained: the position of the local burning surface could be associated at discrete spots on the samples (see A,B, and C in Fig. 6).

$$\bar{r}_{bA-B} = \frac{y_b^B - y_b^A}{t^B - t^A} = \bar{r}_{bC} \qquad (2)$$

the average burning rate between spot B and spot A on the sample was obtained with eq. 2, i.e. by dividing the length between the two points by the time needed by the front to reach point B starting from point A. This average burning velocity was then associated to point C, placed at the middle.

The distance between two measurement spots was chosen to minimize the error to about 2.5%.

A whole distribution of burning rates was obtained for the loaded samples. It was found out that the burning rate was the same as with the unloaded strand burners at spots *without* apparent dewetting, and greatly enhanced at zones with uniform dewetting damage. An even higher apparent increase was recorded at spots with damage patterns 2 and 3.

A continuous 2D map of the burning rate was generated by correlating the r_b values obtained at the measurement points. A typical distribution of burning rate can be observed in Fig. 8. The sample from which it was obtained is shown in Fig. 7. The distribution of burning rates is a fingerprint of the damage distribution on the material sample, just like the material stiffness distribution would be. The region of damage pattern 2 (white circle on Fig. 7) is embedded in a region with diffused dewetting. To confirm the results, undamaged 2D specimens were tested under a mechanical load below the threshold of dewetting; the burning rate proved to be the same as the one obtained from conventional strand burners of undamaged material. Results are shown in Table 2, reporting the average, minimum, and maximum burning rates obtained at spots with “type 1” damage (diffused dewetting). The same data for type 2/3 damage zones are reported in the last line of the table.

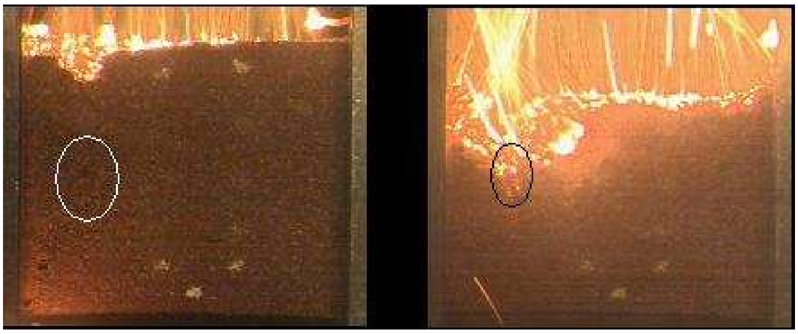

Fig. 7 *One of the 2D specimens showing a “type 2” damage pattern zone (bridged crack) at the centre left. Further portions of the samples have diffused dewetting (type 1), others are undamaged*

Table 2 *Burning rates at 1 atm obtained using samples (10) of mechanically damaged propellant under load.*

Specimen type	Average Damage factor g(ε)[3]	r_b, mm/s	COV, %	min. r_b mm/s	max. r_b mm/s
Strand burners, undamaged propellant	1	1.16	2	1.13	1.19
2D specimens, undamaged	1	1.15	–	–	–
2D specimens, damaged to 30% true strain; type 1 damage patterns - dewetting	0.375	1.47 (+28%)	14.7	1.18	2.32
2D specimens, damaged to 30% true strain; type 2/3 damage patterns - microcracks	0.375	–	–	2.43	4.2 / 9

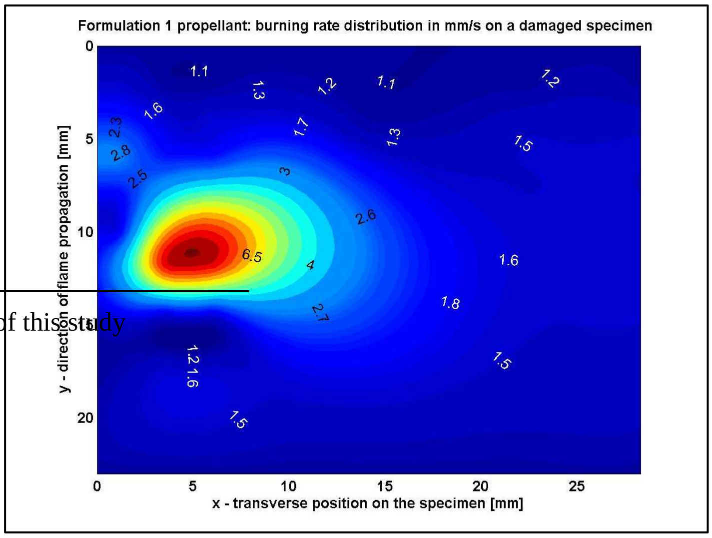

[3] see part II of this study

Fig. 8 *Typical burning rate distribution for the damaged samples under load. The r_b for the specimen of Fig. 8 was at 55 points. A correlation was performed with Matlab, obtaining a 2D map of the burning rate of the material. The numbers and colors on the contour plot display the local burning rate in mm/s*

Final comments

The increase in burning rate for the material zones with a “type 1” damage (diffused particle dewetting) is remarkable and amounts to about **28%** of the burning rate value for the undamaged material. In zones with damage patterns 2 and 3, apparent burning rates of up to 8 times the undamaged values were found. These values are not true burning rates but flame spreading phenomena into small, merely observable cracks. These cracks would be undetected with normal motor diagnostics but their presence might be inferred in future systems with embedded sensors [24 and 25]. Analyzing the videos, a clear distinction can be made between damage pattern 1 material portions and damage pattern 2 and 3 material portions:

– In the first case, only the examination made under the microscope carried out before the test reveals that the material has diffused particle dewetting (Fig.1). During combustion, the flame front proceeds straight and normal, without blurring, and a mere (but remarkable) increase of the rate of propagation of the burning front in the material is recorded.

– In the second case, a small crack is merely observable in the video, and almost as soon as the burning surface reaches the upper crack tip, the flame propagates inside the crack by its entire length. A very high apparent burning rate (4 mm in about 0.5 s) can be associated to this “forward jump” of the burning surface if the length of the crack is divided by the time elapsed from the moment the burning surface reaches the upper crack tip and the bottom of the crack is ignited. It is pointed out that if this time is shorter than the inverse of the frame rate of the camera, this value is not real but a function of the frame rate. Whether the burning rate values associated to propellant with type 2 and type 3 damage patterns can be used as a material property for simulation purposes

using an Eulerian grid fixed on an unflawed grain (regardless of whether bulk mechanical deformation is simulated or not by coupling FEA) depends on the resolution of the grid.
If a single grid cell is larger than the length of a type 2 or type 3 flaw and the material is treated as homogeneous, the burning rate assigned as a material property to the cell should be correspondingly high. If the small crack is detected and the model takes it into account by including a small crack between two neighboring cells, then the neighboring cells should have the same burning rate as undamaged material or a material with a pattern 1 damage assigned as a material property.

Acknowledgement

The help and advise of Prof. Giuseppe Sala, Ms. Rosy Pagano, and Mr. Paolo Bettini (Dept. of Aerospace Engineering, Politecnico di Milano) in conducting mechanical testing is gratefully acknowledged

References

[1] Cain, J., and Brewster, Q., “Radiative Ignition of Fine Ammonium Perchlorate Composite Propellants” Propellants, Explosives and Pyrotechnics, 31, No.4 278-284, Wiley, 2006.
[2] Summerfield, M., and Parker,K.H. ”Interrelations between combustion phenomena and mechanical properties in solid propellant rocket motors”, in “Mechanics and Chemistry of Solid Propellants”, Eringen, A.C. editor,1967.
[3] Murdock, W. “Flow-Structural Interactions in Solid Rocket Motors”, from “Internal Aerodynamics of Solid Rocket Motors”, Special Course held at the Von Karman Institute of Fluid Dynamics, 27-31 May 2002.
[4] Glick, R., Caveny, L., and Thurman, J., “Internal Ballistics of Slotted-Tube, Solid-Propellant Rocket Motors,” Journal of Spacecraft, Vol. 4, No. 4, 1967.
[5] Kuo, K.K., and Kooker, D.E. “Coupling Between Nonsteady Burning and Structural Mechanics of Solid Propellant Grains”, in “Nonsteady Burning and Combustion Stability of Solid Propellants” in AIAA Progress in Astronautics and Aeronautics Series, Vol. 143, De Luca, Price, Summerfield editors, 1992.
[6] Hwang, C., Massa, L., Fiedler, R. and Geubelle, P., “Simulation of convective burning and dynamic fracture in solid propellants”, 38th AIAA/ASME/SAE/ASEE JPC Conference and Exhibit, Indianapolis, Indiana. Paper NO. AIAA 2002-4342.
[7] Smirnov, N.N., and Dimitrienko I.D., „Convective Combustione Regime in a Deformable Solid Fuel with Longitudinal Channels“, Fizika Goreniya i Vzryva, Vol. 22, No.3, pp. -59-67, May-June 1986, Moscow (translation).
[8] Lu, C., and Kuo, K., “Modelling and numerical simulation of combustion process inside a solid rocket propellant crack”, Propellants, Explosives, Pyrotechnics 19, 217-226.

[9] Lu, Y.C., Kuo, K.K., and Wu, S.R. “Crack Propagation Process in a Burning AP-Based Composite Solid Propellant, AIAA 93-2168, AIAA/SAE/ASME/ASEE 29th Joint Propulsion Conference, 28-30 Jun 1993.

[10] Liu, C.: 2002, Fracture mechanics and service life prediction research, Technical Report AFRL-PR-ED-AB-2002-208, Edwards AFB CA Propulsion, Directorate West.

[11] Ramohalli, K.N.R., “Steady State Burning of Composite Propellants under Zero Cross-Flow Situation”, in “Fundamentals of Solid Propellant Combustion” AIAA Progress in Astronautics and Aeronautics Series, vol. 90, Kuo and Summerfield eds., 1984.

[12] Lengellé, G., Duterque, J., and Trubert,J.F. “Combustion of Solid Propellants” from “Internal Aerodynamics of Solid Rocket Motors”, Special Course held at the Von Karman Institute of Fluid Dynamics, 27-31 May 2002.

[13] Agard Advisory Report 350 (AR 350) “Structural Assessment of Solid Propellant Grains”, Propulsion and Energetics Panel Working Group 25, North Atlantic Treaty Organization, Dec. 1997.

[14] Simo, J.C., “On a fully three-dimensional, finite strain viscoelastic damage model: formulation and computational aspects”, Computer Methods in Applied Mechanics and Engineering, Vol.60, 1987.

[15] Shapery, R.A.,“ A Theory of Mechanical Behavior of Elastic Media with Growing Damage and other Changes in Structure” J.Mech.Phys.Solids, Vol. 38, No.2 pp. 251-253, 1990.

[16] Shapery, R.A., “Models for Damage Growth and Fracture in Nonlinear Viscoelastic Particulate Composites”.

[17] Schapery, R.A.,”A Micromecanical Model for Non-Linear Viscoelastic Behavior of Particle-Reinforced Rubber with Distributed Damage, Eng. Frac. Mech., Vol. 25, Nos 5/6 pp.845-867, 1986.

[18] Maggi, F., „Heterogeneity Effects on Composite Solid Propellants“, PhD. Thesis in Aerospace Engineering, Politecnico di Milano, April 2006.

[19] Bencher, C., Dauskardt, R. and Ritchie, R.: 1995, “Microstructural damage and fracture processes in a composite solid rocket propellant“, Journal of Spacecraft and Rockets 32(2), 328–334.

[20] Sandri Tussiwand, G., Saouma, V.E., De Luca, L.T., and Terzenbach R., “Fracture Mechanics of a Solid Rocket Motor using an AP-based Composite Propellant“ draft paper submitted for publication to the Journal of Propulsion and Power, Sept. 2006

[21] Maggi F., Bandera A., Petracca A., De Luca L.T. and Annovazzi A. "Grain processing effects on steady burning rate in small-scale test motors", proceedings of the 9-IWCP congress on „Novel energetic materials and applications“, 14-18 Sep 2003, Lerici, La Spezia, De Luca, Galfetti e R.A. Pesce-Rodriguez editors.

[22] NASA SP-8073, “Solid Propellant Grain Structural Integrity Analysis”, National Aeronautics and Space Administration, Jun 1973.

[23] Fitzgerald, J.E., and Hufferd, W.L., “Handbook for the Engineering Structural Analysis of Solid Propellants”, CPIA Publ. 214.

[24] R.R. Little, H. Chelner, and H.J. Buswell, „Development, Testing and Application of Embedded Sensors for Solid Rocket Motor Health Monitoring“ 37th International Annual Conference of ICT, June 2006.

[25] Sandri Tussiwand, G., Weterings, F.P., Reeling Brouwer, G., and Besser, H.L. ”Application of Embedded Bondline Sensor Technology to a Nozzleless Rocket Motor, 37th International Annual Conference of ICT, June 2006.

[26] Mullins, L. „Softening of rubber by deformation“, Rubber chemistry and technology, 42, 339-362, 1969.

[27] Bueche, F. “Network Theories of Reinforcement”, in “Reinforcement of Elastomers”, G. Kraus ed., Wiley, 1965.

[28] Francis, E.C., and Carlton, C.H., “Some Aspects of Composite Propellant Nonlinear Behavior in Structural Applications”. ICRPG/AIAA 3rd Solid Propulsion Conference, June 1968.

[29] Farris, R.J., ”The Influence of vacuole formation on the response and failure of highly filled elastomers” Trans.Soc.Rheology 12,315-334, 1968.

[30] G. Sandri Tussiwand, F. Maggi, A. Bandera, and L.T. De Luca “Intrinsic Structural-Ballistic Interactions in Composite Energetic Materials Part II – Modeling”**.** International Conference on Non-Isothermal Phenomena and Processes, November, 27 Nov – 01 Dece 06, Yerevan, Armenia.